AUTOMATED LINEAMENT MAPPING FROM REMOTELY SENSED DATA: CASE STUDY OSUN DRAINAGE BASIN, SOUTHWESTERN NIGERIA

Akinwumiju, A. S.[1]; Olorunfemi, M. O.[2] and Afolabi, O[2]

[1]Institute of Ecology and Environmental Studies, Obafemi Awolowo University, Ile-Ife, Nigeria

[2]Department of Geology, Obafemi Awolowo University, Ile-Ife, Nigeria

(Corresponding Author: ojhakin@yahoo.com

(Received: 6th Dec., 2015; Accepted: 4th Feb., 2016)

ABSTRACT

The automatic procedures of PCI LINE and Imagine Objective Line Extraction were adopted to extract lineaments from Landsat OLI imagery (band 6) and Digital Elevation Models (SPOT DEM and ASTER DEM) of Osun Drainage Basin, Southwestern Nigeria. This was with a view to optimally map lineaments within the basin. The optical images were initially subjected to Median filtering in order to edge out all unwanted linear information while preserving the target geotectonic lineaments. Thereafter, the filtered images were subjected to both linear (directional) and non-linear (non-directional) edge enhancement algorithms. The resultant omni-directional and non-directional edge enhanced images were subjected to Object-based Image Analyses, which culminated to lineament map of high accuracy. Subsequently, the resultant composite lineaments were categorized into morphological and geotectonic lineaments based on lithological and hydrological information. Furthermore, borehole data were employed to assess the hydrogeological significance of the geotectonic lineaments. It was observed that the number of lineaments increased with decreased azimuth interval of filtering directions with SPOT DEM giving the highest number of lineament. Directional filtering along N-S and E-W directions proved to be the most efficient in detecting most lineaments within the study area. Forty seven per cent of the composite lineaments were adjudged to be hydrogeologically significant with dominant azimuth directions of NE-SW and NW-SE while minor trends (N-S and E-W) were also represented. The clustering of hydrolineaments and the corresponding lineament intersections coincided with the occurrence of felsic rocks particularly within the upland axis of the study area. Results of this study suggested that the more the input data and the adopted techniques, the higher and more reliable are the resultant lineaments. Moreover, SPOT DEM proved to be the most efficient among the input optical datasets.

Keywords: Remote Sensing, Lineaments, Hydrogeology, Image Processing, Edge Enhancement

INTRODUCTION

O'Leary *et al.* (1976) described lineaments as simple or composite linear features that are aligned in a rectilinear or slightly curvilinear relationship and which differ from the adjacent features and presumably represent the subsurface phenomenon. The term lineament was introduced by Hobbs (1904) to denote the surface signature of the occurrence of brittle tectonic structures such as faults, large-scale fractures and fracture zones. Since then, lineament has been used in various fields especially in groundwater studies (Anisimova and Koronovsky, 2007; Meijerink *et al.,* 2007; Mallast *et al.,* 2011). Lineament was introduced in groundwater context by Lattman (1958) and Lattman and Parizek (1964). Thereafter, many researchers have adopted the technique of lineament mapping and analysis to quantify groundwater resources particularly within the Basement Complex terrain (Greenbaum, 1987; Sander, 1996; Akinluyi, 2013; Bayowa, 2013; Ojo *et al.,* 2015). To prove the applicability of lineaments as indicators of fault/fractured systems and the assumable preferential zones of groundwater accumulation, many authors have compared both features and reported a strong relationship both in shallow and deep aquifers (Salvi, 1995; Sander *et al.,* 1997 Oguchi *et al.,* 2003). The surface expression of geological structures such as faults/fractures, shear zones and foliations are often displayed or represented in the form of lineaments in remotely sensed data such as satellite imageries and Digital Elevation Models (Solomon, 2003). Mapping and analysis of lineaments constitute an integral part of many geo-scientific studies such as tectonics, engineering geology and geomorphology and in the exploration of natural resources such as solid minerals, petroleum and groundwater (Koopmans, 1986; Kar, 1994; Philip, 1996; Mallast *et al.,* 2011). This technique is equally relevant in environmental studies such as mapping of

possible pathways for the transportation of pollutants, identification of suitable locations for dump siting and delineation of suitable sites for earth dams.

Lineaments can be mapped based on fieldwork within a local context. However, lineament mapping is better undertaken on regional basis in order to have extensive perspective of the occurrence of geological structures. In this case, remotely sensed data are inevitable. Overtime, satellite imageries and Digital Elevation Models (DEMs) have been subjected to various digital image processing techniques in order to delineate lineaments (Awoyemi *et al.,* 2005; Sander, 2007; Mallast *et al.,* 2011). Classical approaches to lineament mapping are usually conducted manually (Solomon, 2003; Awoyemi *et al.,* 2005; Akinluyi, 2013; Bayowa, 2013; *Ojo et al.,* 2015). This subjective technique usually results in the production of lineament map that is not reproducible (Wladis, 1999). Thus, manually extracted lineaments are not objective and are equally inefficient in terms of time and cost (Hung *et al.,* 2005; Sander, 2007; Vaz *et al.,* 2008; Mallast *et al.,* 2011). Moreover, lineament mapping would be better appreciated if the results were reproducible. This can only be achieved by adopting any form of automated or semi-automated lineament extraction techniques. Although automated and semi-automated lineament extraction techniques are not new (Moore and Waltz, 1983; Wang and Howarth, 1990); in recent time, high efficient automated and semi-automated lineament algorithms have been introduced (e.g. Segment Tracing Algorithm (STA), Hough Transform, PCI LINE and Imagine Objective Line Extraction Algorithm) (Karnieli *et al.,* 1996; Mallast *et al.,* 2011).

However, it is highly imperative that false lineaments (that represent roads, power lines and other anthropogenic features) are eliminated while geo-tectonic lineaments are preserved (Hung *et al.,* 2005; Mallast *et al.,* 2011). To this end, Median filtering module has been proved to be the most efficient optical image enhancement algorithm that preserves tectonic lineaments (Mather, 2004; Quackenbush, 2004; Arias-astro and Donoho, 2009). Nevertheless, Mallast *et al.* (2011) emphasized the importance of spatial and spectral resolution of remotely sensed data in lineament mapping. In this case, high resolution optical images are more appropriate but with challenges of price-intensive and the tendency of consisting numerous unwanted linear information. On the other hand, medium resolution optical images are more advantageous in terms of their availability at little or no cost (with the exception of SPOT DEM) and the fact that they usually contain less unwanted information. But it is pertinent to emphasize that a coarser resolution would suppress small-scale lineaments. Despite the fact that optical images are widely accepted as appropriate input data for lineament mapping, some authors have emphasized the need for careful assessment of the resultant lineaments (Jordan and Schott, 2005; Arenas Abarca, 2006; Mallast *et al.,* 2011). This is because linear features could be morphologically induced or of tectonic origin. This challenge can be overcome by introducing lithological, hydrological (surface drainage) and hydrogeological information (Solomon, 2003; Mallast *et al.,* 2011).

Osun Drainage Basin (ODB) in Southwestern Nigeria is a watershed that is drained by the sixth order Osun River Network that takes its origin from various perennial streams, which take their courses from Ekiti-Ijesa mountainous region. ODB is the upland northeastern watershed, which is a major donor sub-basin of the much larger Osun-Ogun Drainage Basin in Southwestern Nigeria. The Osun-Ogun River Network is one of the few drainage systems in the Southwestern Nigeria that empties its contents directly into the Gulf of Guinea. Recently, a comprehensive inter-disciplinary-based groundwater potential assessment was carried out across ODB that involved detail integrated hydro-lineament mapping. This study therefore presents the adopted lineament extraction methodology and the evaluation of the delineated lineaments in terms of hydrogeological significance.

The Study Area

ODB lies within Latitudes 7°35'N and 8° 00'N and Longitudes 4°30'E and 5°10'E; in the forested undulating Yoruba Plain of Southwestern Nigeria (Figure 1). The basin (2,194.59 km^2) extends from the upland area of Ekiti State to the low lying area

of Osun State, covering 21 Local Government Areas with projected population of 6.2 million as at December, 2014 (Akinwumiju, 2015). ODB is underlain by the Precambrian Basement Complex that is characterized by both foliated and non-foliated rocks such as quartzite/quartz schist, amphibole schist, mica schist, migmatite, porphyritic granite, biotite granite, pegmatite, granite gneiss, banded gneiss and charnockite (Fig. 2).

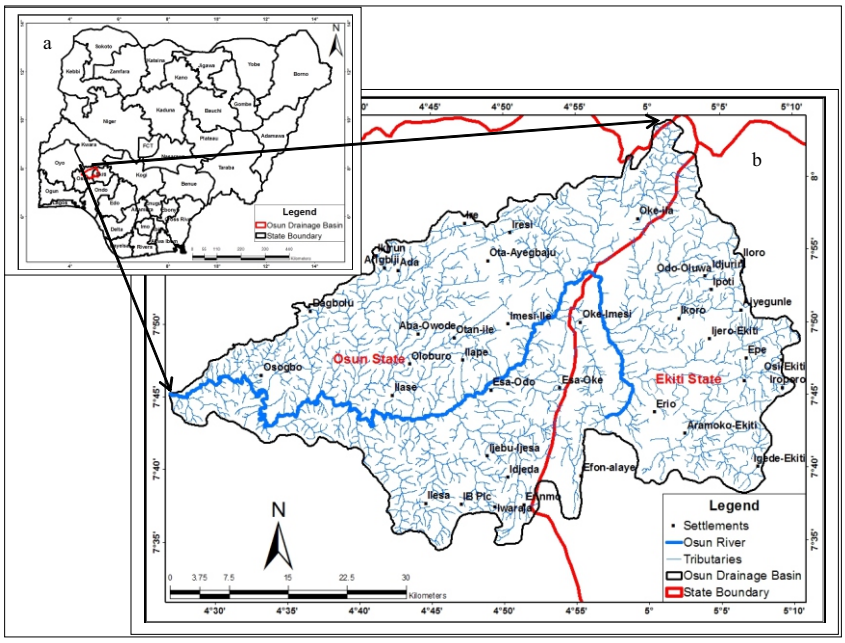

Figure 1: Map of the Study Area showing a): Nigeria's State Boundaries; b): Osun Drainage Basin

Notable geological structures within the study area include Efon Ridge Mountains and the Zungeru-Ifewara Fault Zone that dissect the study area (De Swardt, 1953; Elueze, 1977; Boesse and Ocan, 1988; Oluyide, 1988; Odeyemi *et al.,* 1999; Awoyemi *et al.,* 2005). The study area falls within the zone of extensive regional metamorphism (popularly known as Ilesa Schist Belt), which could probably have resulted to pronounced faulting and fracturing of the bedrocks.

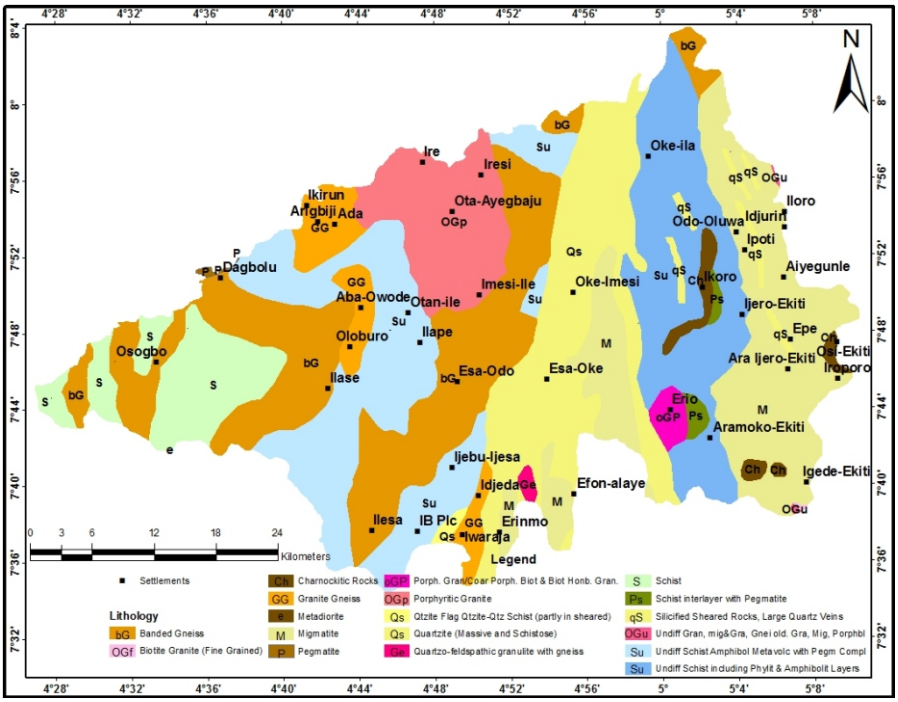

Figure 2: The Geological Map of Osun Drainage Basin (Extracted from NGSA, 2006)

METHODOLOGY

The Nature of the Required Data and Tools

The research endeavors was accomplished by utilizing secondary data, the verification of the reliability of the results was based mainly on the primary data and experience that was gathered during the field investigations. The input data and the sources are presented in Table 1a. The research required the integrated adoption of a number of computer packages that are mostly geoscience specific. Thus, the software and the purposes of employing them are presented in Table 1b.

Analytical Procedures

Two types of remotely sensed datasets were utilized in this study (Table 1a). These datasets include:

(i) Satellite Imagery

- Landsat OLI/TIRS data (30 m resolution) path/row (190/055) acquired in February, 2014

Landsat 8 carries two different earth-observation scanners, the Operational Land Imager (OLI) operating in the visible, NIR and SWIR portions of electromagnetic spectrum and the Thermal InfraRed Scanner (TIRS) imaging in the thermal infrared. Both are "pushbroom" scanners rather than opto-mechanical. The OLI has two new wavebands; band 1 is in the "deep blue" portion of the spectrum for water studies, while band 9 is in the atmospheric absorption window for better discrimination of cloud and data quality assessment. The other bands are re-numbered (Table 2), and the near infrared (ETM band 4, OLI band 5), SWIR (ETM band 5, OLI band 6) and SWIR (both ETM and OLI band 7) are all narrower in OLI. The 15-metre resolution panchromatic channel (Band 8) is also spectrally narrower in OLI, excluding the NIR portion of the older panchromatic band. The single thermal channel in ETM is split into 2 bands in TIRS (bands 10 and 11), which provides an enhanced potential for geological discrimination based on differential thermal emissivities of rocks. The main geological implications of the differences between OLI/TIRS and the older ETM+ are that lithological and structural discrimination should be better with OLI because of the narrower band widths, and that the two thermal channels should permit crude lithological discrimination using ratioing techniques. The raw Landsat data were processed in Erdas Imagine 2013 environment and filtered band 6 image (band 6 of Landsat OLI/TIRS) was generated.

Table 1a: Required Secondary Data and Expected Sources.

S/No.	DATA	PRODUCTION DATE	SOURCES
1	ASTER Digital Elevation Model (DEM)	2009	Ministry of Economy, Tra de, and Industry (METI) of Japan /United States National Aeronautics and Space Administration (NASA) Database.
2	Geological Map	2006	Nigeria Geological Survey Agency, Abuja
3	Topographical Map.	1966, 2010	Office of the Surveyor General of the Federation, Abuja, Nigeria.
4	Spot Digital Elevation Model (DEM)	2012	Office of the Surveyor General of the Federation, Abuja, Nigeria.
5	Landsat Imagery.	2014	Global Land Cover Facility.
6	Spot5 Imageries.	2009, 2012	Office of the Surveyor General of the Federation, Abuja, Nigeria.

Table 1b: Required Software and Instrumentation

S/No.	SOFTWARE	USES
1	ArcGIS 10x	Geo-database Creation, Spatial Modeling, Vectorization, Spatial Data Integration, Geospatial Analyses, 3D Modeling.
2	Erdas Imagine 2013	Pre-lineament Extraction Image Processing, Image Processing.
3	ENVI 5.0	Image Enhancement, Filtering, Band Maths & Ratioing.
4	PCI Geomatica 14.0	Lineament Extraction, 3D Modeling.
5	Rockwork 16.0	Lineament Azimuth-Frequency Modeling.

(i) Remotely sensed Digital Elevation Models (DEMs)
- Spot DEM (20 m resolution) acquired in 2012
- ASTER DEM (30 m resolution) acquired in 2011

The characteristics of the DEMs are presented in Table 3.

Table 2: OLI and TIRS Spectral Bands Compared to ETM+ Spectral Bands (USGS, 2015)

Landsat-7 ETM+ Bands (μm)			Landsat-8 OLI and *TIRS* Bands (μm)		
			30 m Coastal/Aerosol	0.435 - 0.451	Band 1
Band 1	30 m Blue	0.441 - 0.514	30 m Blue	0.452 - 0.512	Band 2
Band 2	30 m Green	0.519 - 0.601	30 m Green	0.533 - 0.590	Band 3
Band 3	30 m Red	0.631 - 0.692	30 m Red	0.636 - 0.673	Band 4
Band 4	30 m NIR	0.772 - 0.898	30 m NIR	0.851 - 0.879	Band 5
Band 5	30 m SWIR-1	1.547 - 1.749	30 m SWIR-1	1.566 - 1.651	Band 6
Band 6	60 m TIR	10.31 - 12.36	*100 m TIR-1*	*10.60 – 11.19*	Band 10
			100 m TIR-2	*11.50 – 12.51*	Band 11
Band 7	30 m SWIR-2	2.064 - 2.345	30 m SWIR-2	2.107 - 2.294	Band 7
Band 8	15 m Pan	0.515 - 0.896	15 m Pan	0.503 - 0.676	Band 8
			30 m Cirrus	1.363 - 1.384	Band 9

The ASTER Global Digital Elevation Model (ASTER GDEM) is a joint product developed and made available to the public by the Ministry of Economy, Trade, and Industry (METI) of Japan and the United States National Aeronautics and Space Administration (NASA). It was generated from data collected from the Advanced Space-borne Thermal Emission and Reflection Radiometer (ASTER), a space-borne earth observing optical instrument. The first version of the ASTER GDEM, released in June 2009, were generated using stereo-pair images collected by the ASTER instrument on-board Terra. The improved GDEM (second version) that was released in October 17, 2011, added 260,000 additional stereo-pairs, improving coverage and reducing the occurrence of artifacts. The refined production algorithm provided improved spatial resolution, increased horizontal and vertical accuracy, and superior water body coverage and detection. The version two ASTER GDEM maintains the GeoTIFF format and the same gridding and tile structure as that of version one, with 30-meter postings and 1 x 1 degree tiles. Version two shows significant improvements over the previous release. However, it is found that the data contains anomalies and artifacts that will impede effectiveness for direct use (without any post-production processing) in any application other than mere visualization.

An important objective of preliminary ASTER GDEM validation efforts was to characterize the ASTER GDEM in terms of specific features, such as artifacts and residual anomalies, that may affect the overall accuracy of the dataset, impede its use for certain applications, or just render it cosmetically unappealing. Indeed, it was determined that the ASTER GDEM does contain residual anomalies and artifacts that degrade its overall accuracy, represent barriers to effective utilization of the GDEM for certain applications, and give the product a distinctly blemished appearance in certain renditions (AGVT 19,

2009). Particularly for areas where the stack number is small, where persistent clouds are an issue, and where no replacement DEM was available, residual cloud-related anomalies exist in the ASTER GDEM. Much more troublesome than residual cloud anomalies, however, are a variety of pervasive artifacts that are clearly related to linear and curvilinear boundaries between different stack number areas. Such artifacts appear as straight lines, "pits," "bumps," "mole runs," and other geometric shapes. Anomalous elevations associated with these artifacts can range from 1 m or 2 m to more than 100 m. However, statistically, the ASTER GDEM appears generally to meet its pre-production estimated vertical accuracy of 20 m at 95 per cent confidence, globally. Some tiles have substantially better than 20 m accuracy, and some tiles have substantially worse than 20 m vertical accuracy. Therefore, in spite of its shortcomings, the ASTER GDEM is a very useful product for many applications, including those requiring a true global DEM. Raw ASTER DEM data were processed and mosaicked into a single large tile.

The SPOT DEM precision product was fully derived from the reference three-dimensional database, which chiefly comprises SPOT High Resolution Stereoscopic (HRS) data covering pre-defined regions of interest. SPOT HRS was planned to cover at least 30 million square kilometers by June, 2008 but currently, SPOT DEM is available for more than 100 million square kilometers of land area across the globe. SPOT DEM precision is the sole DEM in the market providing detailed information on both the identification and localization of residual errors (artifacts) inherent to automatic correlation computation. This capacity proves SPOT DEM precision to be the ideal for Uncrewed Reconnaissance Vehicle (UAV), missiles and aircrafts on-board database, as well as mission planning for military operation and armament industry. However, the acquisition of SPOT DEM attracts costs as it is strictly for commercial purpose. Nevertheless, its accuracy, precision, and resolutions make SPOT DEM an attractive elevation data in the domain of earth sciences. Minor processing was also carried out on the clipped Spot DEM that has already been partially processed from the source.

Table 3: Characteristics of SPOT DEM and ASTER DEM

CHARACTERISTICS	SPOT DEM	ASTER DEM
Platform/Sensor	SPOT6/HRS	Terra/ASTER
Organization	SPOT/FNSMA	METI/NASA
Year of Acquisition	2012	2011
Resolution	20 m	30 m
Coverage	**>** 100 million km^2	>90% of the Earth
Data Format/Encoding	GeoTiff/16bit	GeoTiff/16bit
Availability	On request at a cost	Free to all users
Datum	EGM 96	EGM 96
Vertical Accuracy	19 m	20 m
Planimetric Accuracy	8 m	11 m

Both DEMs (ASTER DEM and Spot DEM) and band 6 of Landsat8 were prepared for the automated lineament extraction procedure. Pre-processing activities include geometric correction and spectral analyses of the remotely sensed datasets. The raster data were co-registered to the same projected coordinate system and were later clipped with the template of the study area.

Hydro-Lineaments Extraction

The study adopted a knowledge-based system for the identification of geomorphic and tectonic photo-lineaments. These led to the derivation of an edge map using appropriate selected linear feature extraction algorithms and the assignment of those edges into geomorphic and tectonic

lineaments using spatial/contextual, spectral and semantic identification criteria and the construction of final hydro-lineament map. The stages of this methodology are presented below.

Data Processing

Landsat imagery and Digital Elevation Models of the study area were geometrically co-registered with Geological Map and scanned Topographic Map of the study area (with a scale of 1:50,000) and geodetically transformed into the Transverse Mercator Projection WGS84 Datum (Zone 31N). The DEMs and band 6 of the Landsat Imagery were selected for the implementation of the image-based Edge Detection Algorithms. These remotely sensed data were initially contrast-stretched using a linear transform in order to achieve a visually better image for input into the Edge Detection Algorithms. Two different Digital Elevation Models were utilized in this study. They include ASTER DEM (30 m resolution) and SPOT DEM (20 m resolution). In order to remove residual anomalies and artifacts, the DEMs were subjected to smoothing filter before further analysis. Various pixels filter sizes were adopted and Median filter was employed in the smoothing filtering process. Thereafter, the best output was selected for further analyses. A set of second order linear filter in 4 main directions (N; NW; W; SW) and 8 cardinal directions were applied using various kernel sizes (3×3, 5×5, 9×9, 12×12) to detect edges within the DEMs and pre-processed band 6 of Landsat imagery. On the basis of comparative analysis, 9×9 kernel size was selected. Likewise, a set of selected non-linear filters (Prewitt and High Pass) were applied on the DEMs and the Landsat band 6. All the directional images for each input surface were analyzed on a pixel-by-pixel basis and merge into one omni-directional image, keeping only the maximum value of each pixel and the resultant omni-directional images and selected non-linear filtered images were prepared for further analyses. The knowledge-based lineament extraction procedure is presented in Figure 3. The omni-directional images and non-linear filtered images were subjected to Object-Based Image Classification in Imagine Objective and PCI Geomatica environments.

Imagine Objective Procedure: A minimum of 30 training pixels per class were chosen in order to ensure an accurate classification result. In the classification, focus was on two classes: (1) adjacent pixels of high values representing edges and thus topographic features and (2) background pixels representing areas without edges. The resulting probability image (with metric values of 0 to 1 per pixel) was subjected to "threshold and clump" procedure by defining an adequate threshold that separated both classes. Due to the fact that probability image strongly depends on the chosen training samples, different thresholds were iteratively applied and the best threshold was adopted. To clean up the irregularities that were associated with object-based lineament extraction, mathematical morphological closing (where a dilation operation is performed followed by erosion operation) was implemented to close the gaps within an object or between near object and concatenated erosion removed single and not connected pixel. In return, almost explicitly connected pixels that represented discrete topographic edges returned. "Centerline Convert" algorithm was applied on the simplified raster-objects in order to generate lines representing the center of the longest axis of the object. Based

on the integrity of the output lineaments, other knowledge-based operations were performed in order to arrive at a map that displayed linear structures with length and orientation-metrics.

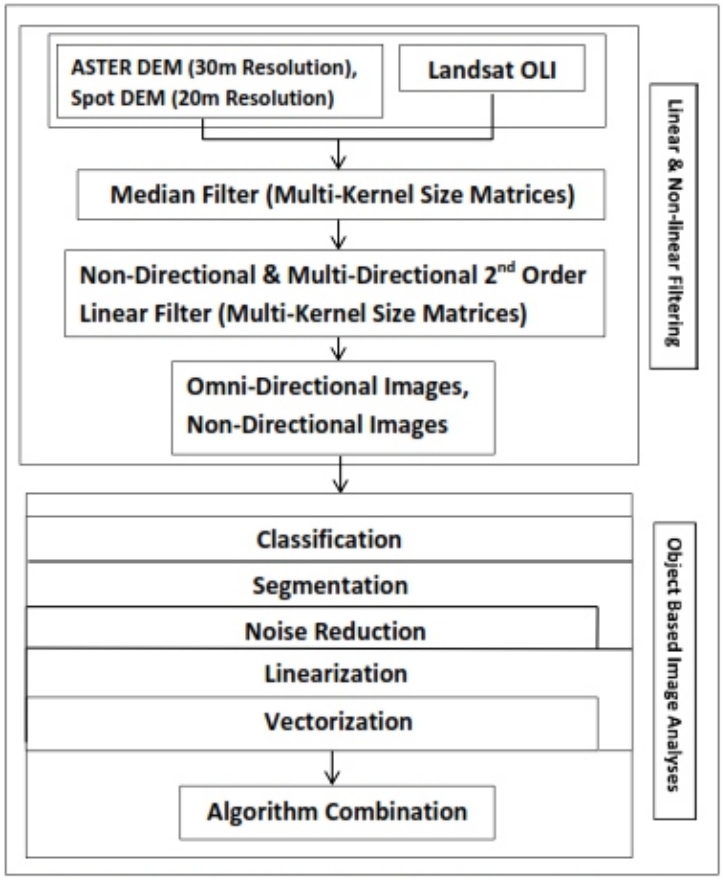

Figure 3: Workflow of the adopted Methods for the Semi-Automated/Automated Extraction of Lineament (After Mallast *et al.*, 2011)

PCI LINE Procedure: The basic approach of PCI LINE is similar to Object-based approach. The only difference is the fact that PCI LINE is based on the robust Canny Edge Detection Algorithm, which filters with a Gaussian filter that depends on the chosen moving window size from which the gradient is subsequently computed. In this case, the pixels that did not represent a local maximum were suppressed. The next step binarized the image based on a threshold value, and a thinning algorithm was then applied. This process was completed with vectorization to extract lines known as lineaments. The defining parameters and the corresponding adopted values are presented in Table 2.

Table 2: The Adopted Parameters for the LINE Algorithm

S/No	Parameters	Code	Values
1	Filter Radius	RADI	60
2	Edge Gradient Threshold	GTHR	10
3	Curve Length Threshold	LTHR	60
4	Line Fitting Error Threshold	FTHR	3
5	Angular Difference Threshold	ATHR	15
6	Linking Distance Threshold	DTHR	10

To obtain a complete and complementary lineament map, the three sets of lineament results (extracted from SPOT DEM, ASTER DEM and Lansat8 band 6) were combined and identical lineaments were singularized in ArcGIS 10.3 environment. Drainage system, topographic and geological information (maps) were introduced in order to differentiate extracted lineament into geological (true structural origin) and morphological (mainly morphological origin with possible structural background). The processes involved in the derivation of information on the drainage system and geology are further described below.

The lithological boundaries contained in the digital geological map of Osun Drainage Basin were inferred and compared to the lineaments. In this case, where a lithological boundary displays similar orientation with a given lineament, it is most likely such lineament reflect the lithological boundary and therefore has to be evaluated as structural lineament. In order to have reliable comparable basis, the most efficient optical dataset (SPOT DEM) among the datasets that were adopted for knowledge-based lineament mapping, was used for the calculation of the drainage system of the study area. Thus, the eight-direction (D8) hydrological flow model incorporated into ArcGIS, was applied in this study. Due to the disparity often noticed between the real drainage network and the automated model, the drainage network was manually extracted from published topographical maps and a mosaicked high resolution multispectral imagery (Spot5 satellite imagery, 2009) of the study area. The two models were compared in order to achieve the best result. The resultant drainage network was projected to a predetermined planar coordinate system and was utilized to isolate the morphologically induced lineaments within the study area. In order to verify the reliability of the adopted automated lineament procedure, final hydrolineament map was compared with an existing lineament map of the study area.

RESULTS AND DISCUSSION

Extracted Lineaments

The lineaments extracted from the omni-directional enhanced SPOT DEM (Figure 4a) is presented in Figure 4b. The number of lineaments delineated from SPOT DEM was the highest (Table 3), arguably due to its improved spatial and spectral resolution compared with other digital datasets utilized in this study. The analysis of the rose diagrams (Figure 5) showed that SPOT DEM is more efficient in terms of lineament length and frequency definition.

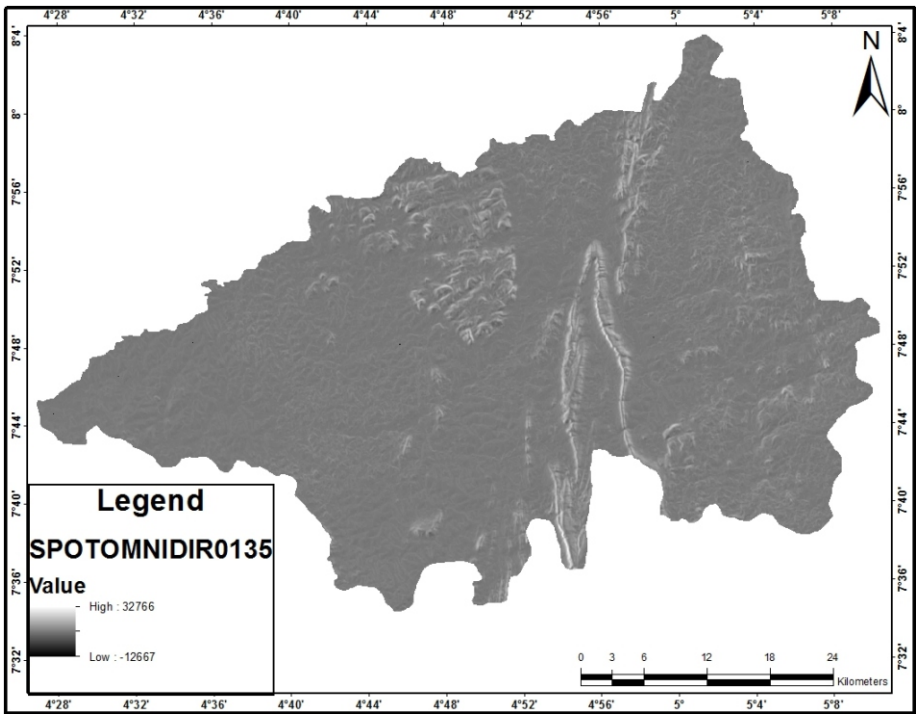

Figure 4a: 4-Cardinal Omni-directional Enhanced Images generated from SPOT DEM

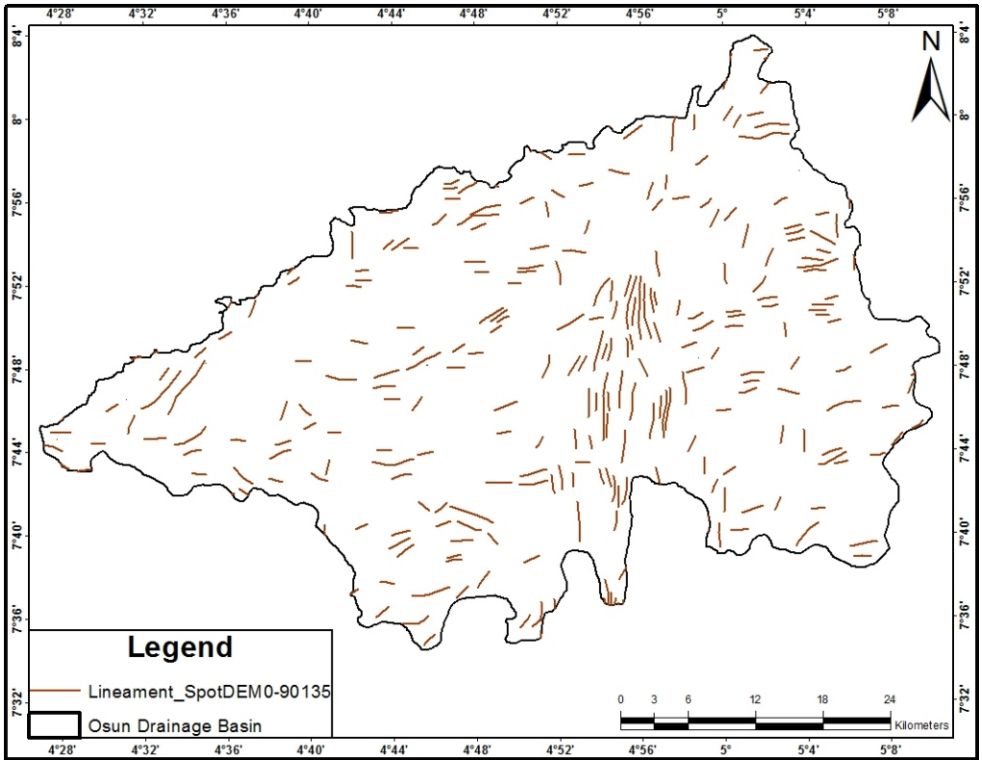

Figure 4b: SPOT DEM-based Lineament Map

Table 3: Summary Statistics

Lineament	Population	Minimum	Maximum	Sum	Mean	Standard Deviation
ENHANCEMENT METHODS						
Prewitt	201	0.081	7.40	361.43	1.80	0.87
High Pass	258	0.072	3.94	391.47	1.52	0.50
APPROACH						
OBIA	12,426	0.000029	2.83	1,251.92	0.1	0.13
PCI LINE	290	0.011	6.10	482.10	1.66	0.73
CARDINAL DIRECTIONS OF FILTERING AND DATA TYPES						
Spot (0-135)	290	0.011	6.10	482.10	1.66	0.73
Spot (0-360)	237	0.03	7.74	429.52	1.81	0.99
Landsat (0-135)	80	0.39	3.82	170.11	2.13	0.58
Landsat (0-360)	87	0.33	4.43	200.26	2.30	0.68
ASTER (0-135)	143	0.02	5.94	348.10	2.43	0.87
ASTER (0-360)	138	0.37	9.03	352.12	2.55	1.13
FINAL OUTPUTS						
Morphologic	300	0.72	5.10	601.45	2.00	0.76
Geotectonic	747	0.50	8.52	1,566.10	2.1	0.97
Composite	1035	0.50	8.52	2145.95	2.1	0.92
Hydrolineament	492	0.081	5.92	837.68	1.7	0.78

For instance, the 15°-75° trending lineaments that were suppressed in ASTER DEM and Landsat image-based lineament maps were adequately represented in SPOT DEM-based lineament maps (Figure 5). Detail observation of the lineament maps revealed twin lineaments (having the same orientation) that were only delineated in the Landsat OLI omni-directional enhanced (Figure 6a) image-based lineament map (Figure 6b). Although more than 90 percent of the lineaments were adequately represented in the SPOT DEM-based lineament maps, some lineaments that were well defined in omni-directional enhanced ASTER DEM (Figure 7a)

and Landsat image-based lineament maps (Figures 6b and 7b) were suppressed in the SPOT DEM-based lineament maps. This development underscores the merit of adopting multi-source datasets in delineation of lineaments, particularly in regions of complex environmental characteristics.

Two distinct linear omni-directional images (i.e. 0-135 and 0-360) were produced and subjected to automated and semi-automated lineament extraction procedures. The first (which comprised the N-S, NE-SW, E-W and NW-SE directional filtered images) yielded the highest number of lineaments in both SPOT DEM and ASTER DEM-based lineament maps (see Table 3). However, the highest number of lineaments were recorded for the 8-cardinal omni-directional enhanced Landsat OLI image compared to the 4-cardinal omni-directional filtered Landsat OLI image. Moreover, it was discovered that lineament lengths were higher for all the 8-cardinal omni-directional enhanced images of all the optical datasets (SPOT DEM, ASTER DEM and Landsat OLI band 6), and this might account for the reduced number of lineaments delineated from DEMs' 8-cardinal omni-directional images (see Table 3). The observed difference between the satellite imagery and Digital Elevation Model may be attributed to different mode of acquisition of the digital datasets as well as the nature of the information they were primarily designed to acquire.

In addition to the directional filtering, two non-linear methods (Prewitt and High Pass) were also adopted for image enhancement. Higher numbers of lineaments was recorded for the directional filtered images while Prewitt filter module was more efficient in defining upper band of lineament length compared to High Pass filter module (see Table 3).

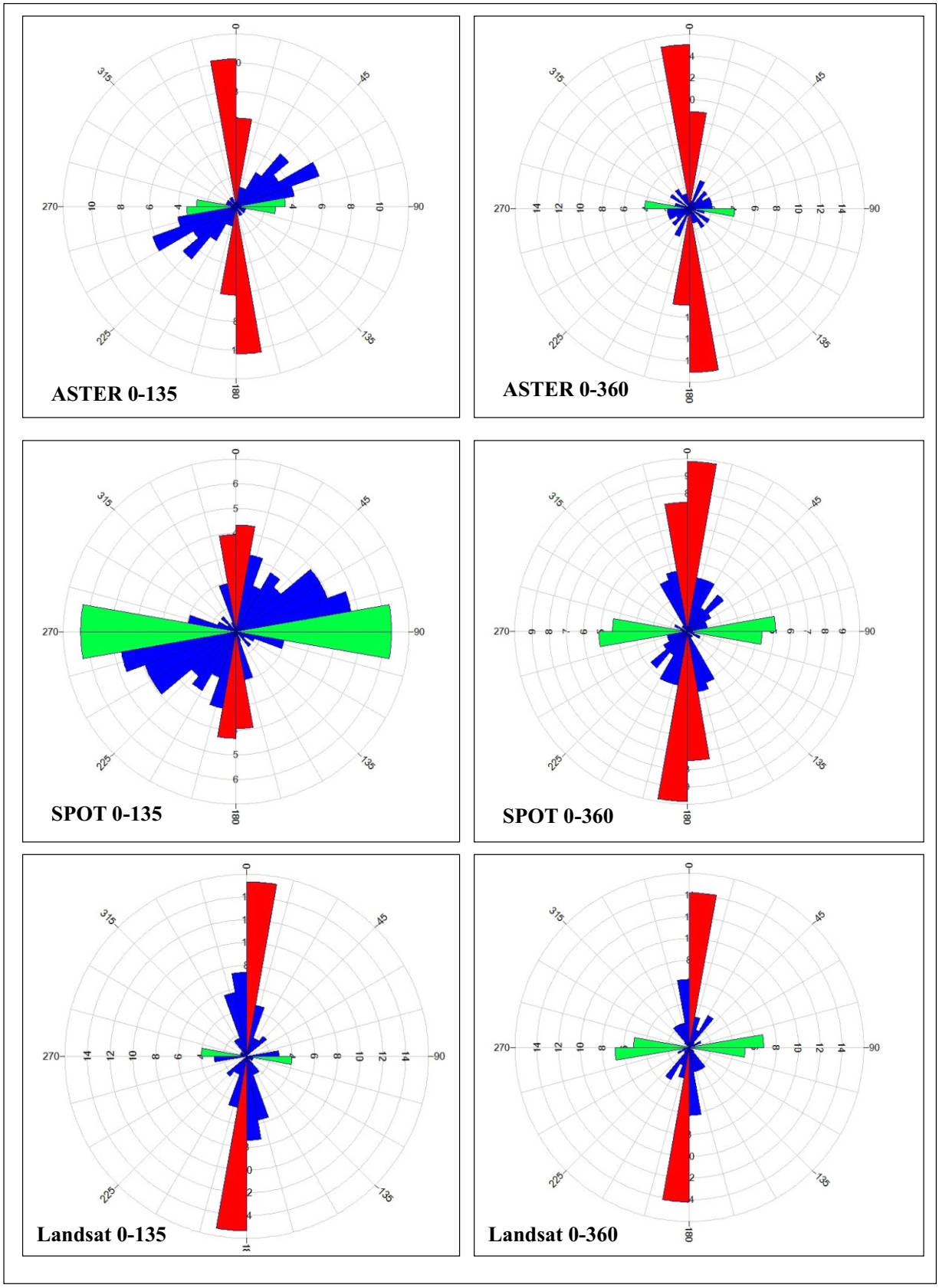

Figure 5: Rose Diagrams of Lineament Generated from Multi-source Data

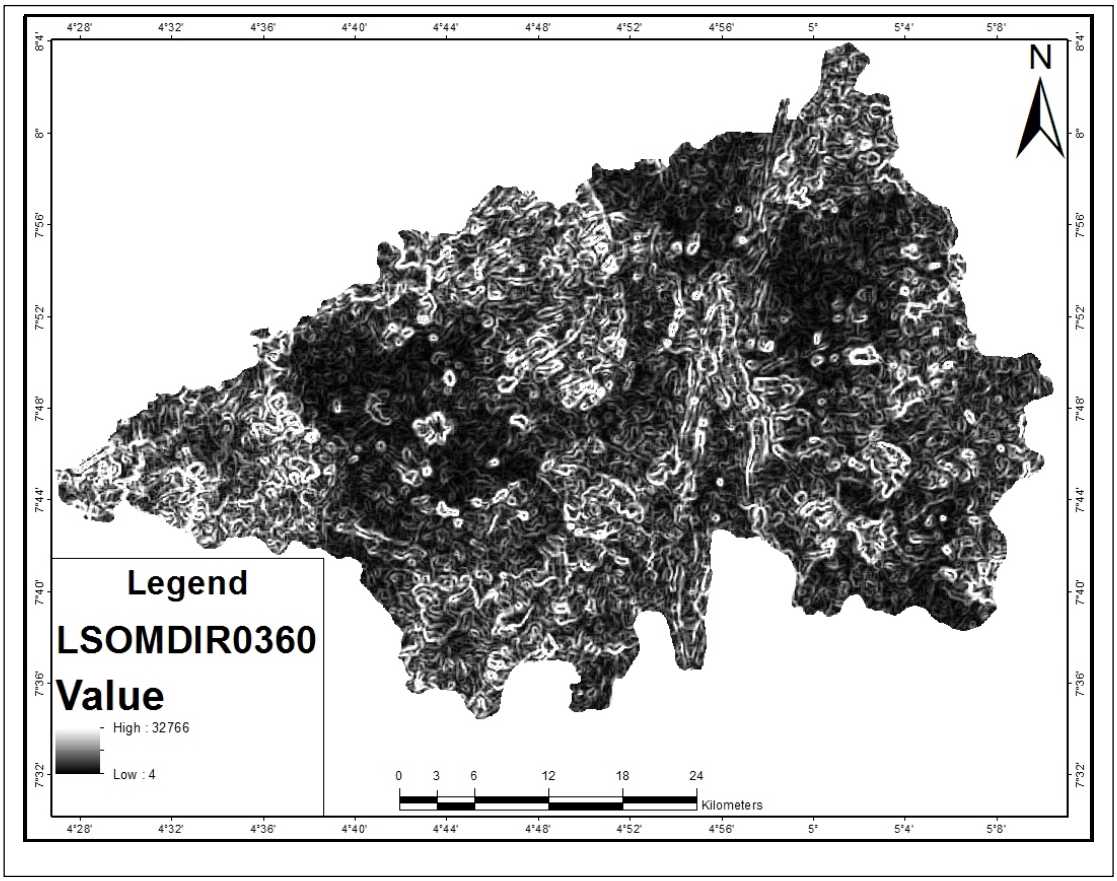

Figure 6a: 8-Cardinal Omni-directional Enhanced Images generated from Landsat8 Band 6

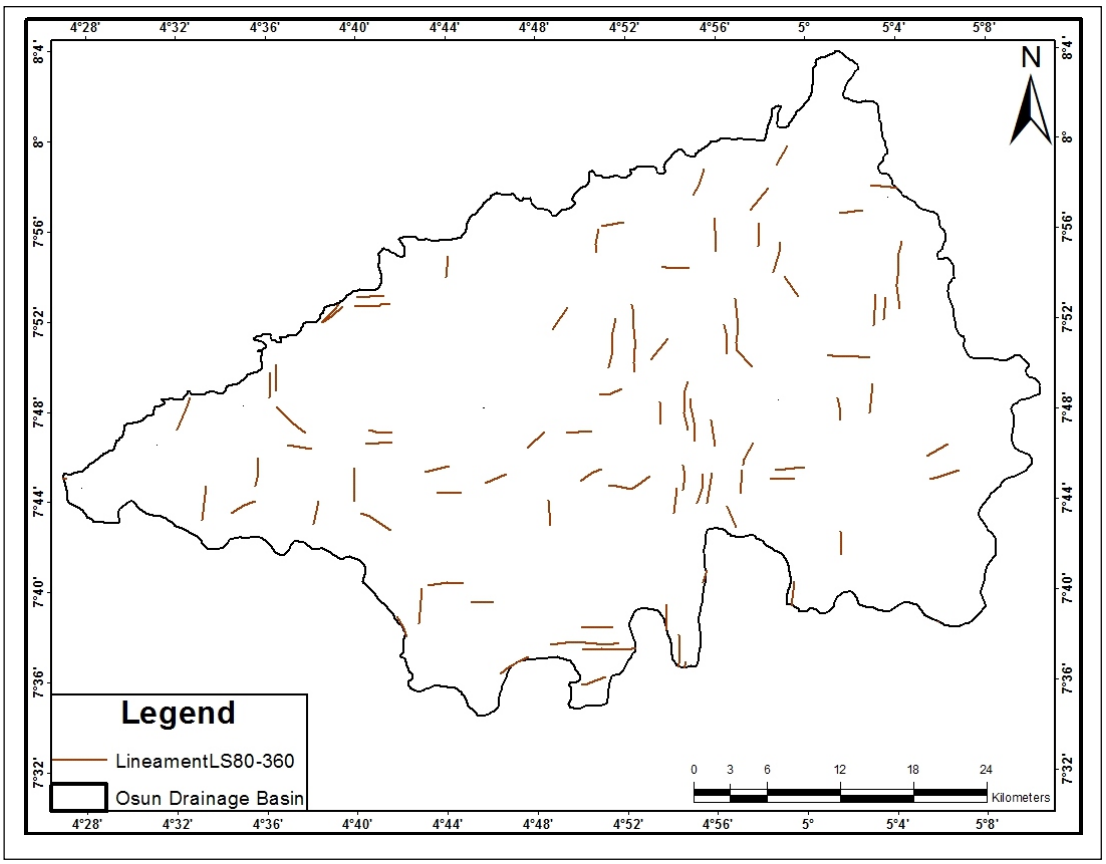

Figure 6b: Landsat-based Lineament Map

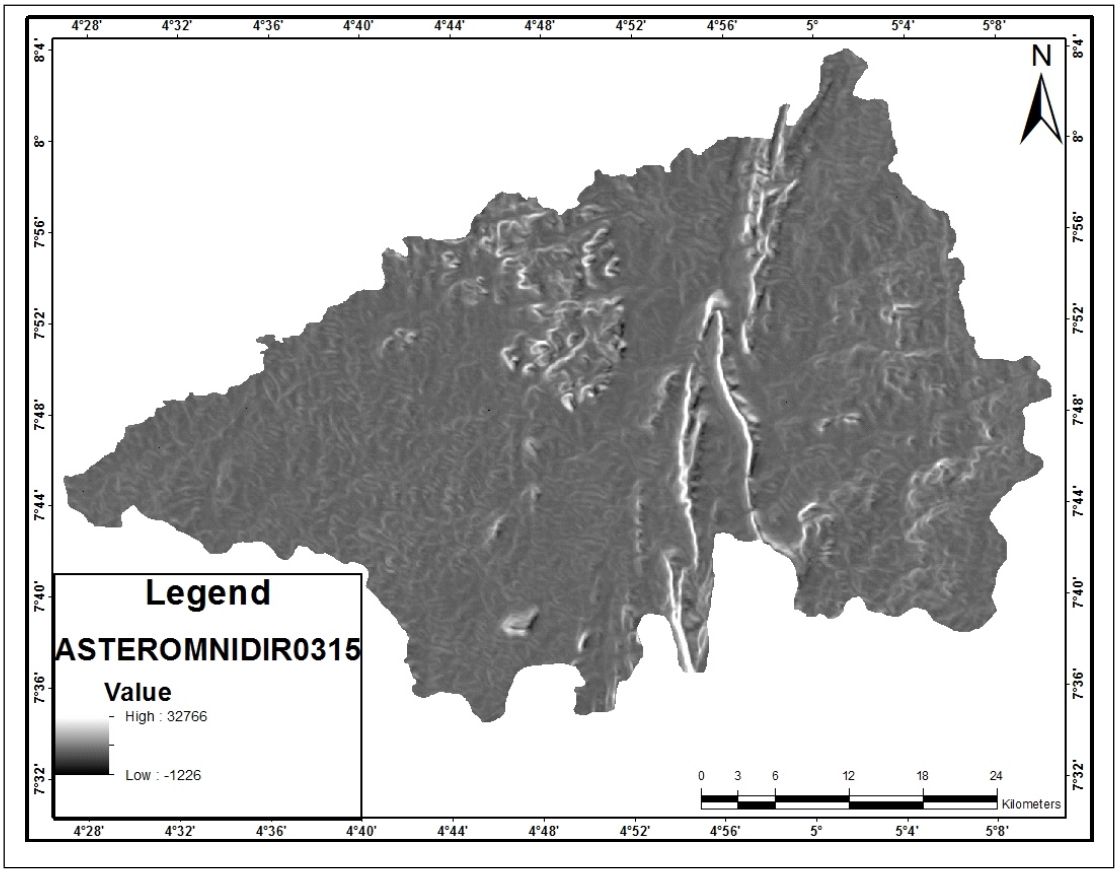

Figure 7a: 4-Cardinal Omni-directional Enhanced Images generated from ASTER DEM

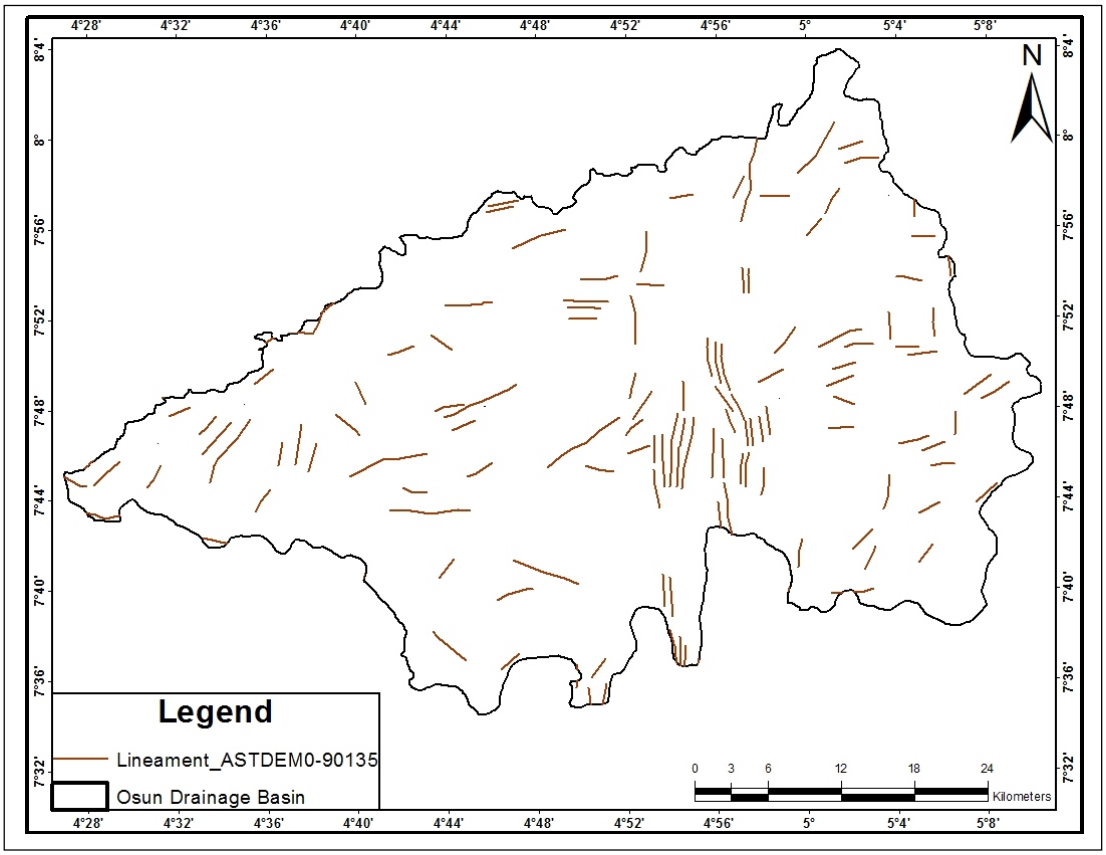

Figure 7b: ASTER DEM-based Lineament Map

The NE-SW (0°-5°) and NW-SE (345°-360°) trending lineaments were adequately represented in all lineament maps generated using all the three methods (Directional, Prewitt and High Pass). However, rose diagrams showed that certain trends (such as the 45°-75° trending lineaments) were almost completely suppressed in the non-linear filtered image-based lineament maps (Figures 8). Comparative assessment of the rose diagrams showed that 285°-345° trending lineaments were poorly represented in all the lineament maps generated in this study. Lineament length was higher in High Pass enhanced image-based lineament map (Figure 9a) than in the Prewitt enhanced image-based lineament map (Figure 9b). The rose diagrams indicate similar performance ability and lineament azimuth direction for the two non-linear filter methods. Generally, it was discovered that the directional filter module is more efficient in terms of image enhancement for lineament delineation.

The highest number of lineaments was recorded for the Imagine Objective procedure; however, 61.5 percent of the 1,252 km total lineament length represented unwanted information (mostly the peaks of elevated landforms) (Table 3). In this case, the output lineaments had to be subjected to editing in order to eliminate the unwanted lineaments. It was discovered that the range of Imagine Objective lineament length was very small; hence the high number of delineated lineaments. A notable advantage of the Imagine Objective procedure is its efficiency in selective orientation-based lineament extraction (Figure 8). All the delineated lineaments in the Imagine Objective-based generated lineament map were adequately represented in the PCI LINE-based lineament map. Although, the preferred margin of the lineament lengths could be determined in both Imagine Objective and the PCI LINE procedures, it is simple and easier in the later compared to long procedure involve in the former. However, the flexibility of the Imagine Objective procedure that allows users to view sub-modular outputs and to make amendments is advantageous compared to the black box approach of the PCI LINE module. Nevertheless, the speed and the efficiency of PCI LINE module makes it a better choice compared to the Imagine Objective Procedure. Experience from this multi-technique analysis of multiple datasets showed that the higher the number of the adopted techniques and utilized datasets, the higher the reliability of the resulted hydro-lineaments.

Lineament Interpretation

The composite lineament map derived from the integration of various lineaments that were extracted from SPOT DEM, ASTER DEM and Landsat OLI data is presented in Figure 10. The geotectonic lineament map that was prepared from the composite lineament map is presented in Figures 11. The frequency-rose diagrams and the characteristics of the composite lineaments and geotectonic lineaments are presented in Figure 12 and Table 3 respectively. The frequency and trends of lineaments are shown in the rose diagrams. The azimuth sector size (class interval) is 10 degrees and length is cumulative for all lineaments within each sector (i.e. azimuth direction). Seventy one percent of the composite lineaments were categorized as geotectonic lineaments while 29 percent represent the morphologic lineaments (Figure 13a) with possible tectonic origin. The characteristics and the frequency-rose diagrams of the morphologic lineaments and the structurally controlled channels are presented in Table 3 and Figure 13b respectively.

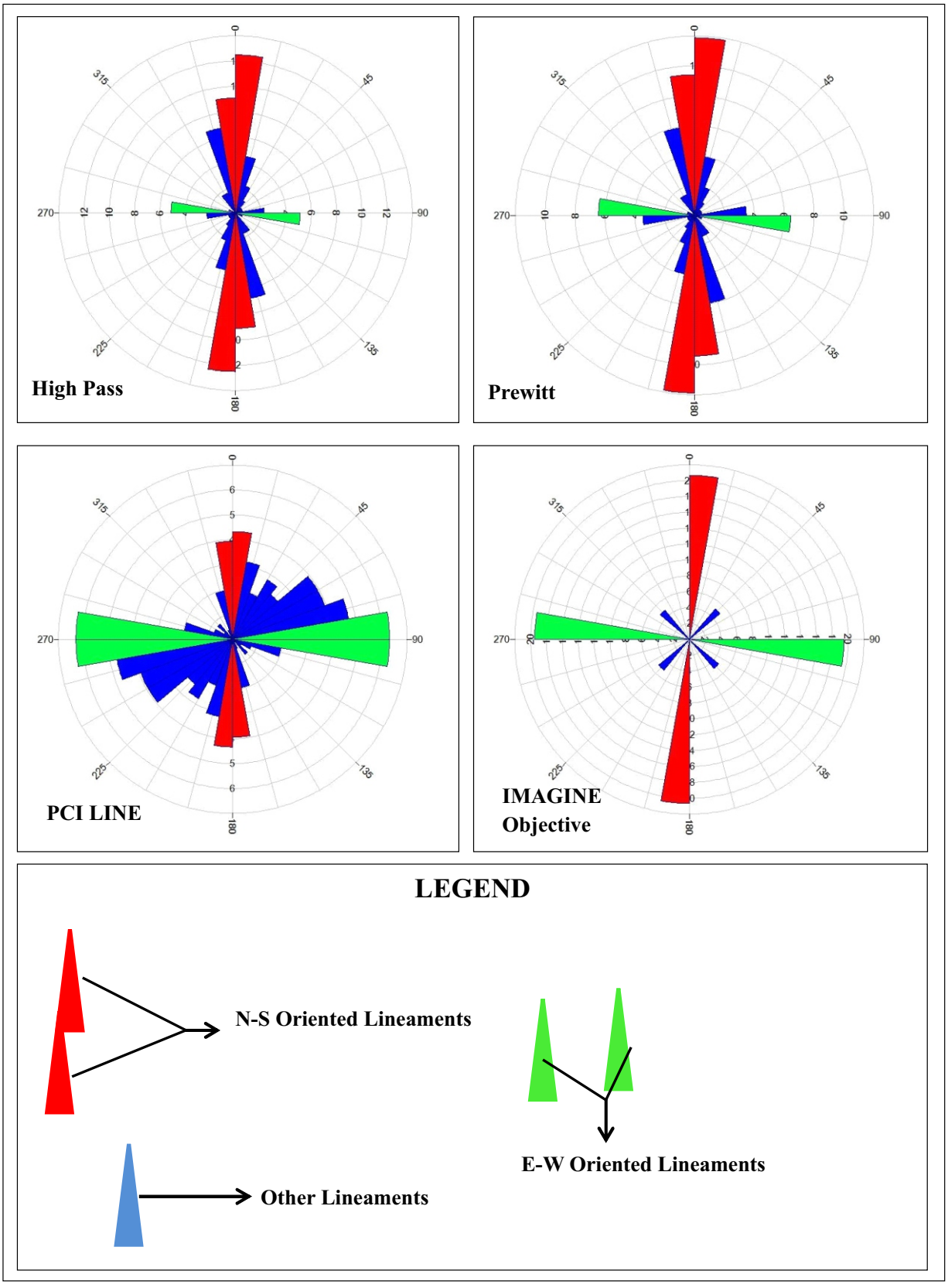

Figure 8: Rose Diagrams of Lineament Generated from various Methods

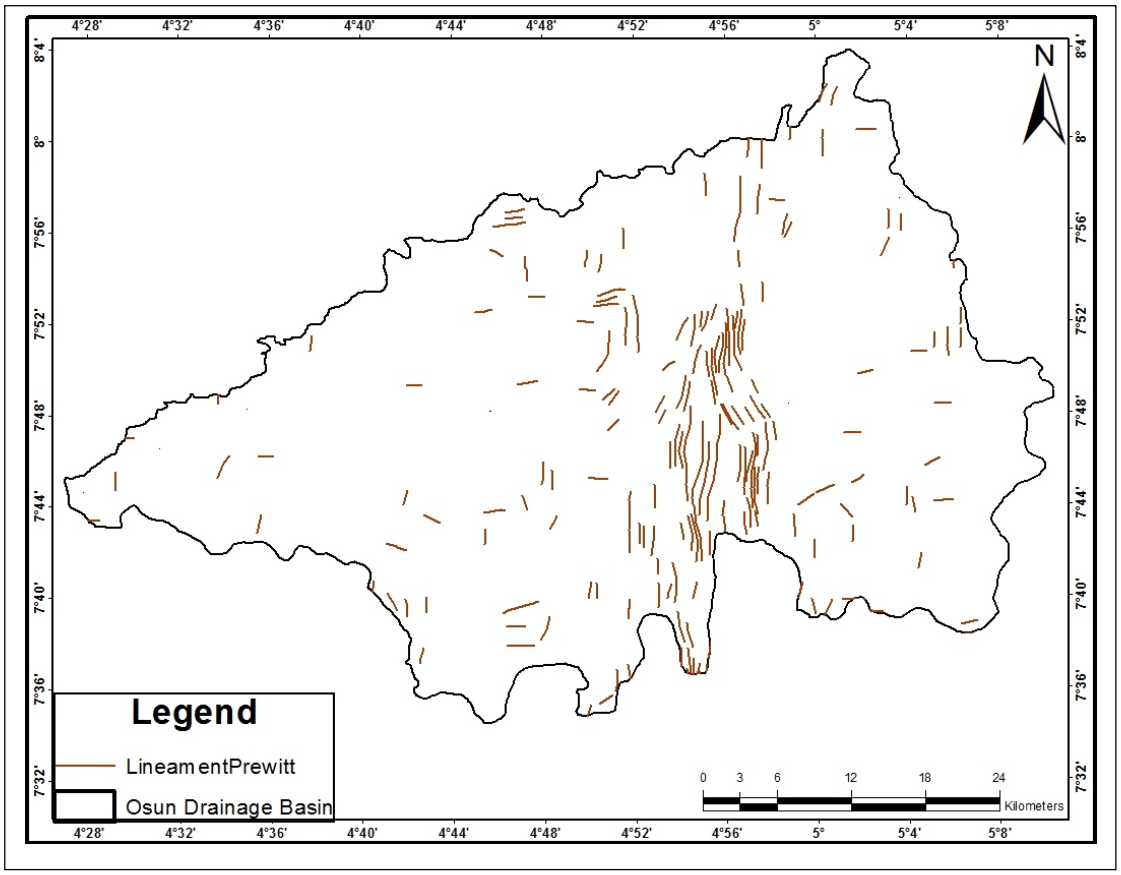

Figure 9a: Prewitt Enhanced Image-based Lineament Map

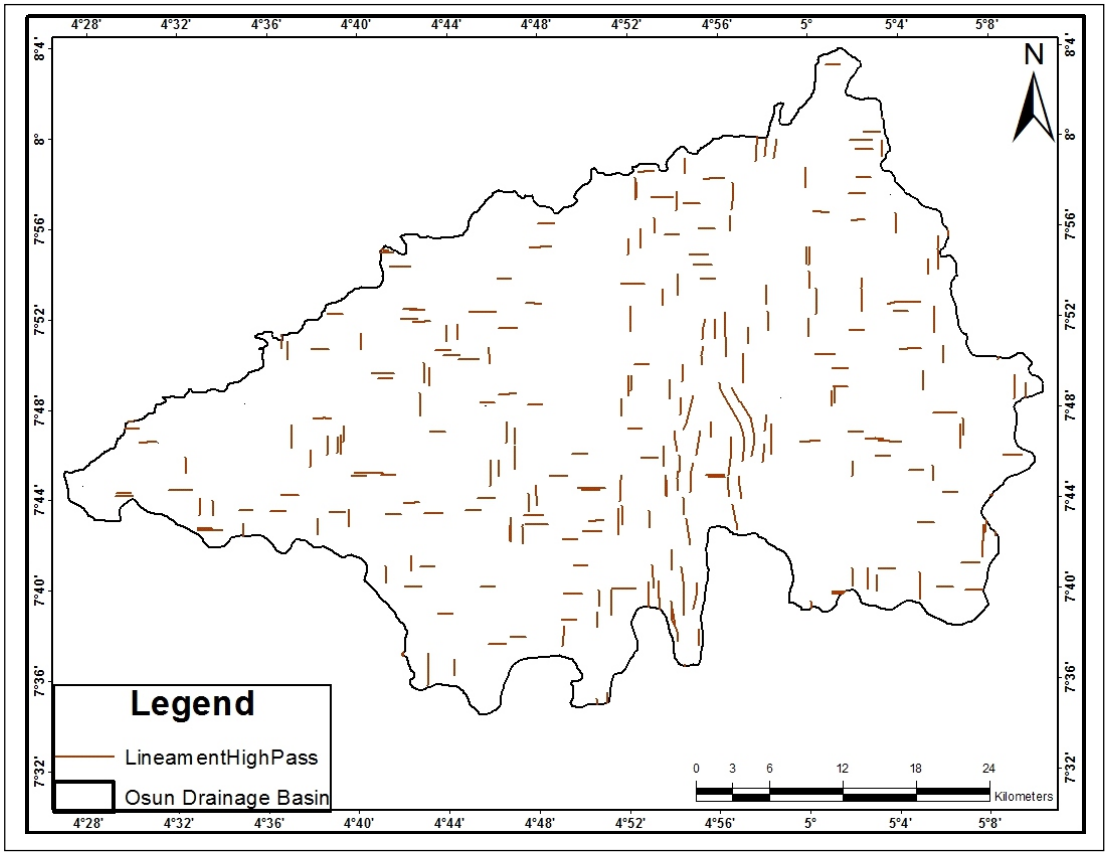

Figure 9b: High Pass Enhanced Image-based Lineament Map

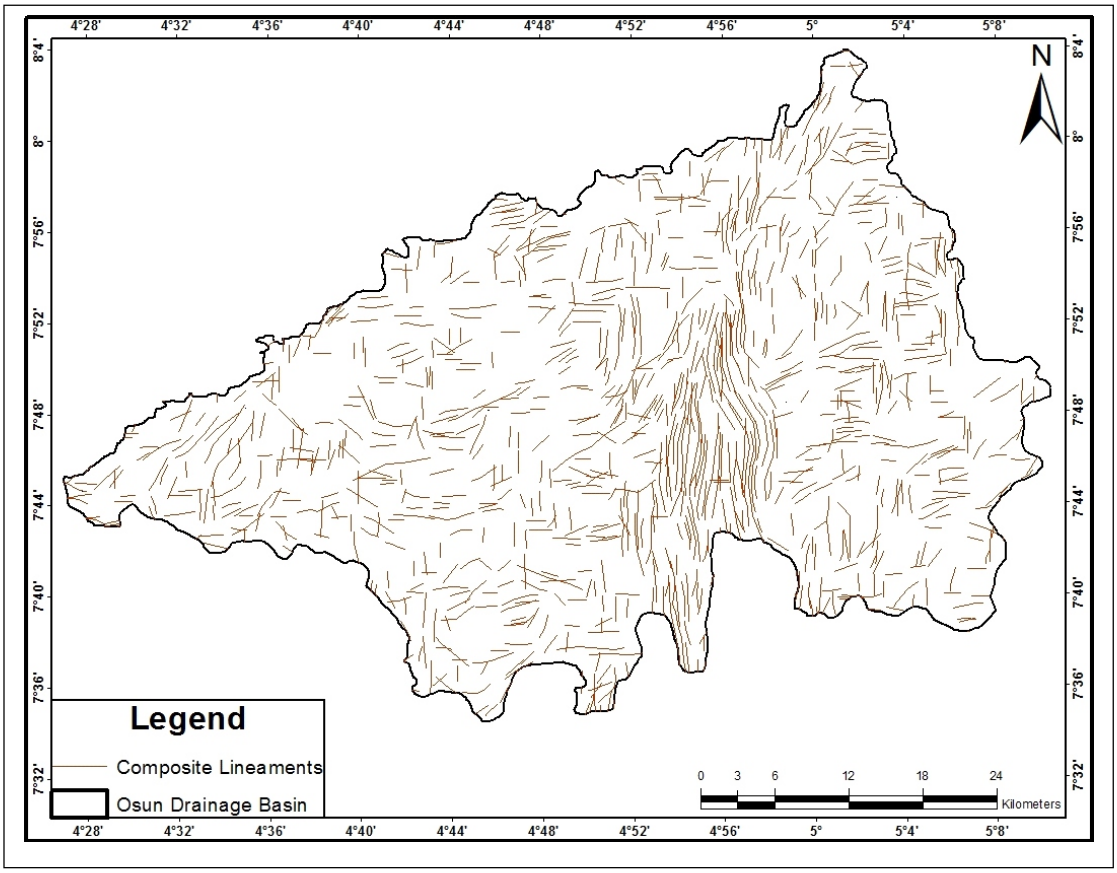

Figure 10: Composite Lineament Map

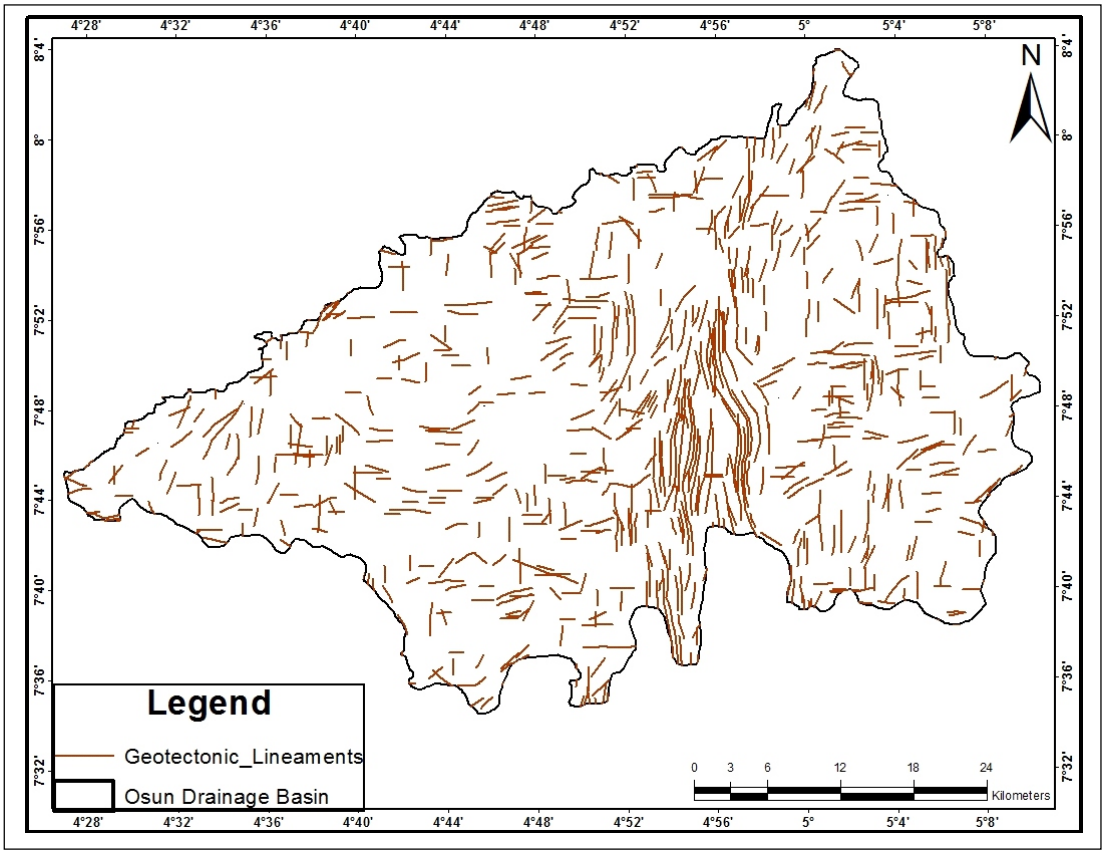

Figure 11: Geotectonic Lineament Map

The orientation of delineated composite lineaments is predominantly N-S (0°-5°) followed by near E-W (75°-90° and 270°-285°) orientations. The minor trends include 30°-45°, 60°-75° and 345°-360°.

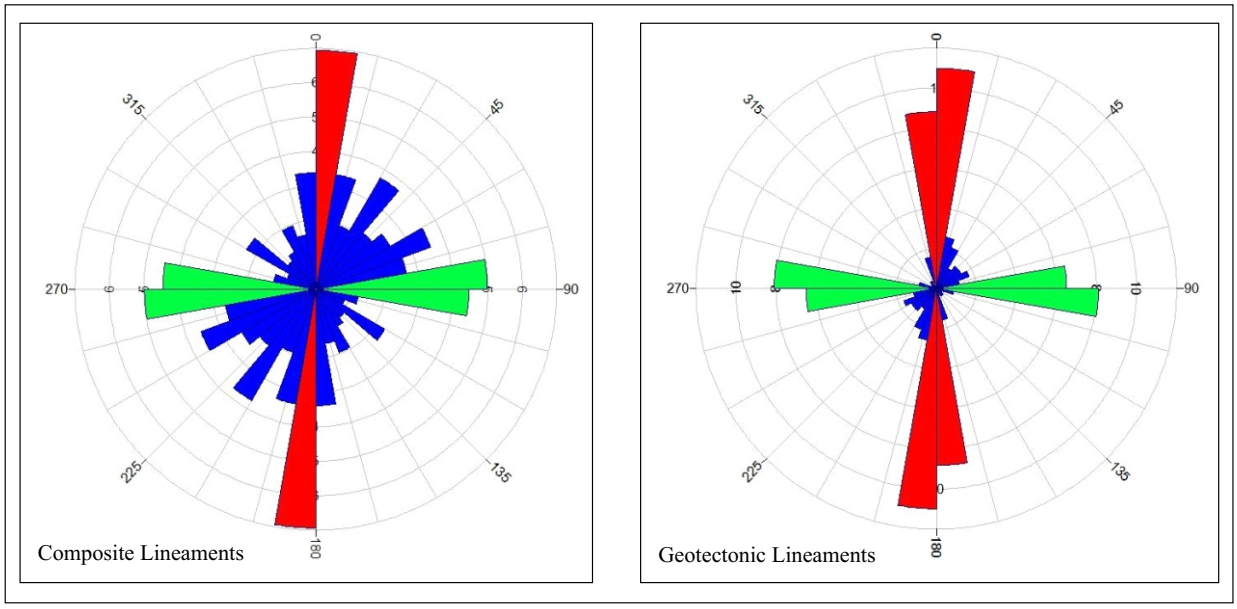

Figure 12: Frequency-Rose Diagrams of Composite and Geotectonic Lineaments

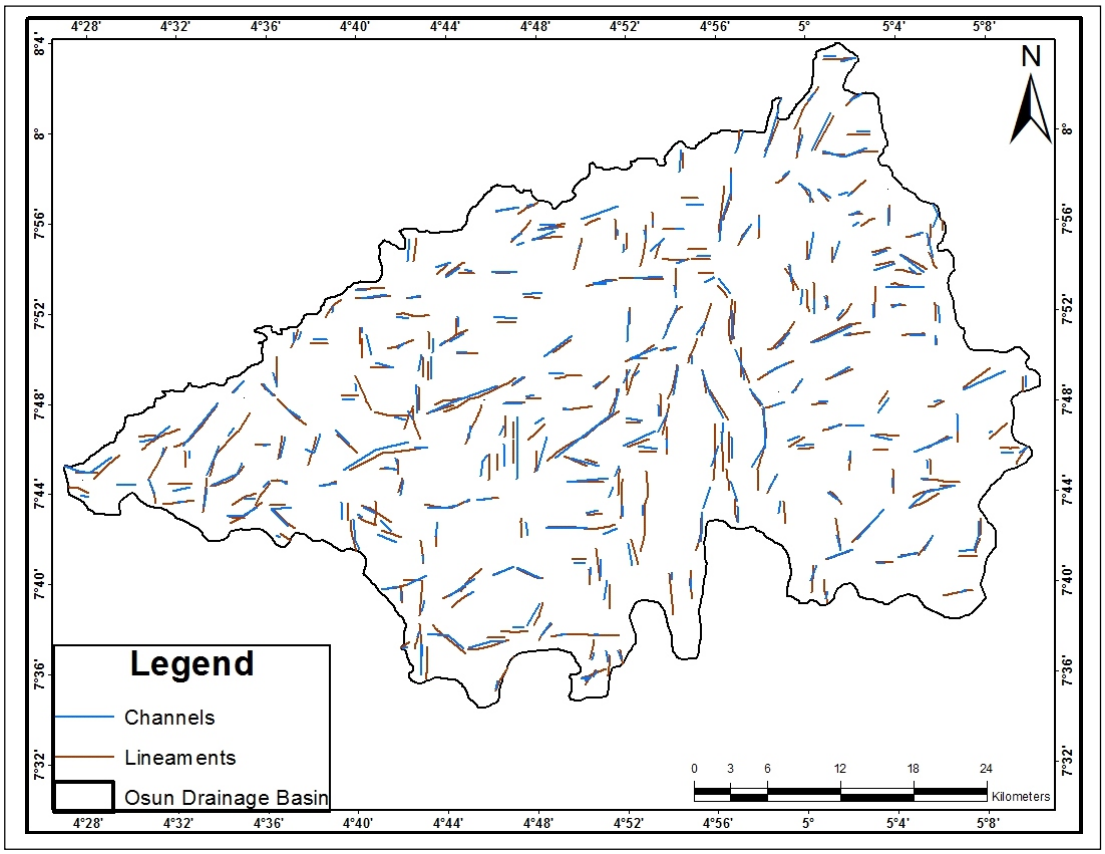

Figure 13a: The Lineament Map Showing Structurally Controlled Channels and the Associated Fault Lines in the Study Area *(a): The Rose Diagram showing the Azimuth Directions of the Structurally Controlled Channels (b)): The Rose Diagram showing the Azimuth Directions of the Associated Fault Line*

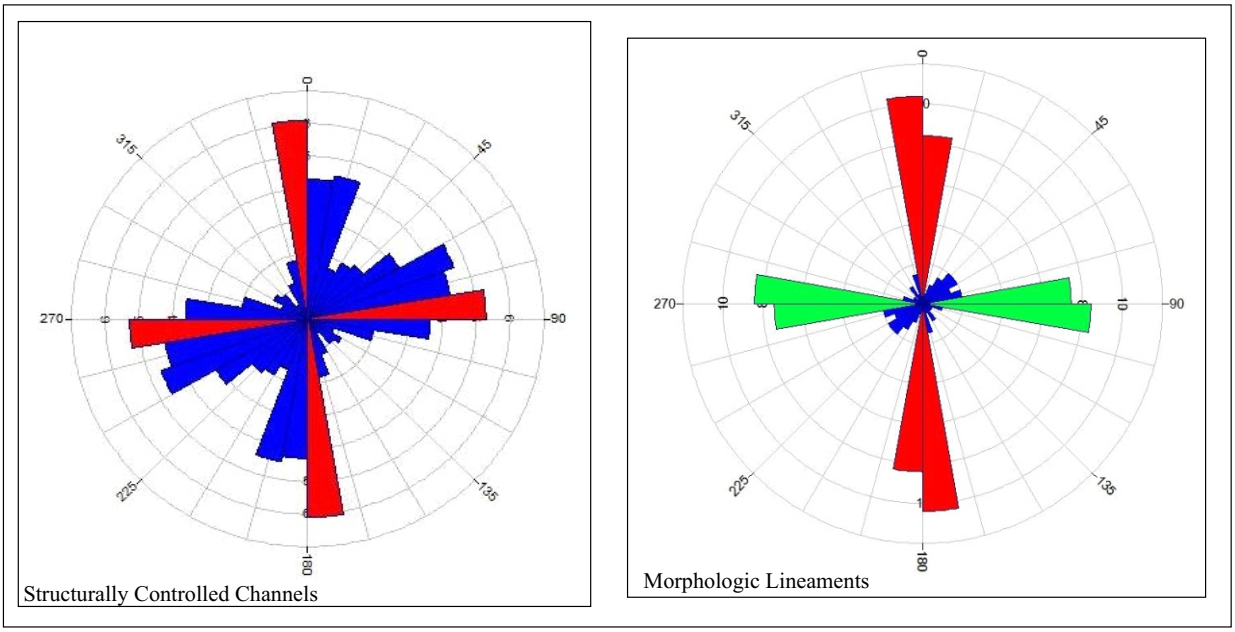

Figure 13b: Frequency-Rose Diagrams of Structurally Controlled Channels and Morphologic Lineaments

Hydrogeologically Significant Lineament

The isolated hydrogeologically significant lineaments and lineament intersections are presented in Figure 14. The characteristics of the hydrolineaments are given in Table 3. Based on various analyses, only 47.5 percent (representing 39 percent of the total length of the composite lineaments) of the total number of the composite lineaments was adjudged to be hydrogeologically significant. As in the case of the geotectonic lineaments, rose diagram indicated that the approximately N-S (345°-0°-5°) oriented lineaments were the most prominent. Also, the near E-W (75°-90° and 270°-285°) oriented lineaments were adequately represented while the (15°-75°) were suppressed (as in the case of geotectonic lineaments) compared to the composite lineament map where these lineaments were adequately represented. The observed pattern of hydrolineament orientations indicate complex and heterogeneous occurrence of groundwater within the study area. Further analyses suggested that the 0°-5° oriented lineaments (that occurred parallel to the Efon Ridge Mountains) indicated the Zungeru-Ifewara Mega Fault while the 75°-90° and 270°-285° oriented lineaments represented major faults that could be sources of highly prolific aquifers within the study area.

Automated procedure showed that there were 114 hydrolineament intersections (cross points) within the study area. Observed spatial pattern of the hydrolineament cross points displayed three clusters (Fig. 14), which were noticed within sub-basins underlain with quartzite (schistose) and porphyritic granite as well as where lithological boundaries concentrate. Thus, the observed pattern indicated strong relationship between geological structures and lithology within the study area. The pattern and orientation of hydrolineaments and hydrolineament cross points gave a visual expression of groundwater occurrence and groundwater flow pattern within the study area. In this case, the pattern of fault lines exerts more influence on groundwater accumulation, movement and flow direction within a typical Basement Complex terrain.

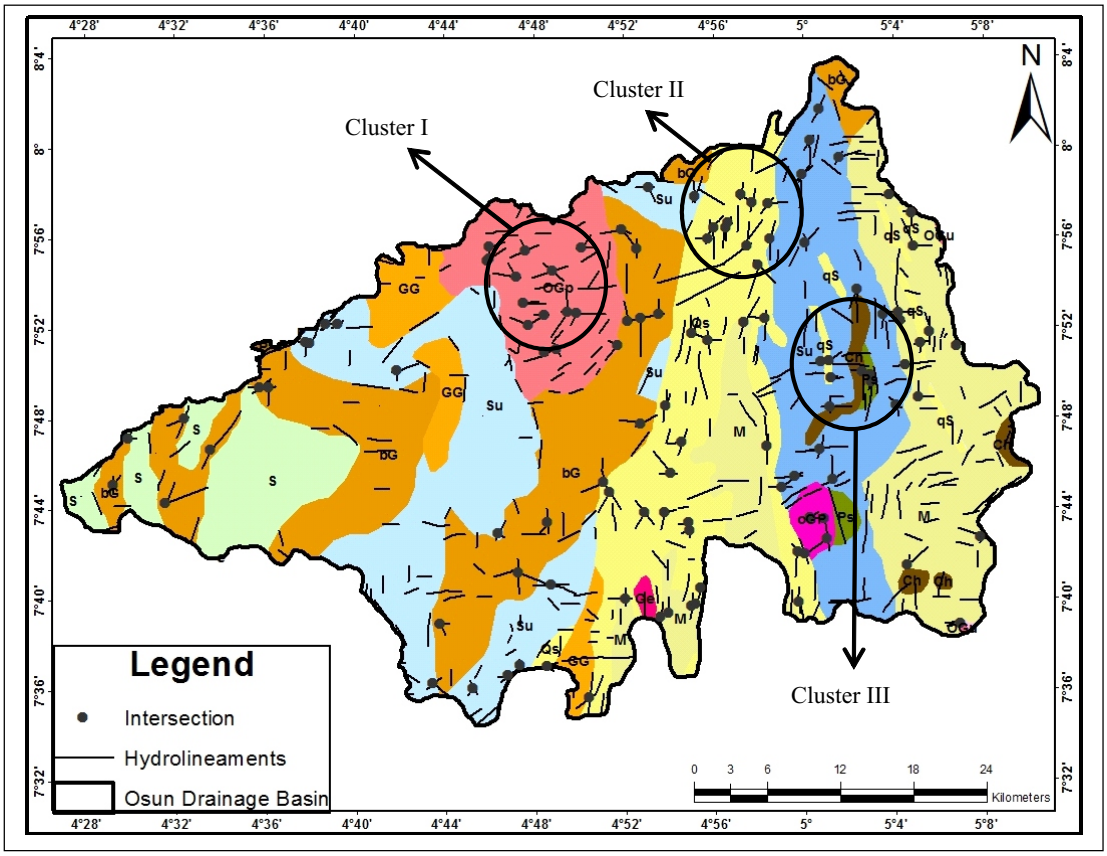

Figure 14: Hydrolineaments and Lineament Intersection Map Superimposed on the Solid Geology

Figure 15a presents the published Lineament Map and the rose diagram of the observed strikes within the study area is presented in Figure 15b. It was observed that the major strikes include the NE-SW (30°-45°) and approximately N-S (345°-360°) while the near E-W trends were not represented. Close observation revealed that Zungeru-Ifewara mega fault (0°-5° trending lineaments) was represented in the existing lineament map and the one produced in this study. Likewise, NE-SW (30°-45°) and N-S (345°-360°) trending lineaments were adequately represented in the existing lineament map and the newly generated lineament map. The pattern of frequency-azimuth direction of the existing lineaments and newly delineated lineaments is presented in Table 4. Result showed that NE-SW trends constitute the major lineament strike both in the existing (60%) and newly generated (62.19%) lineament maps while N-S trending lineaments constitute 40% and 33.34% of the existing lineaments and the newly generated lineaments respectively. On the other hand, the E-W trending lineaments that were relatively represented on the newly produced lineament map were absent in the existing lineament map (see Figure 15b and Table 4). This disparity might be attributed to the efficiency of the automated lineament extraction procedure adopted in this study, which have resulted in the delineation of a new set of lineaments in the study area. Also, it is pertinent to mention that the existing lineament map only present the summarized lineaments that depict major structures that have been confirmed on the ground. Nevertheless, the existing lineament map agrees with the newly generated lineament map to a great extent as revealed by the observed spatial pattern of lineaments and frequency-azimuth direction of both sets of lineaments.

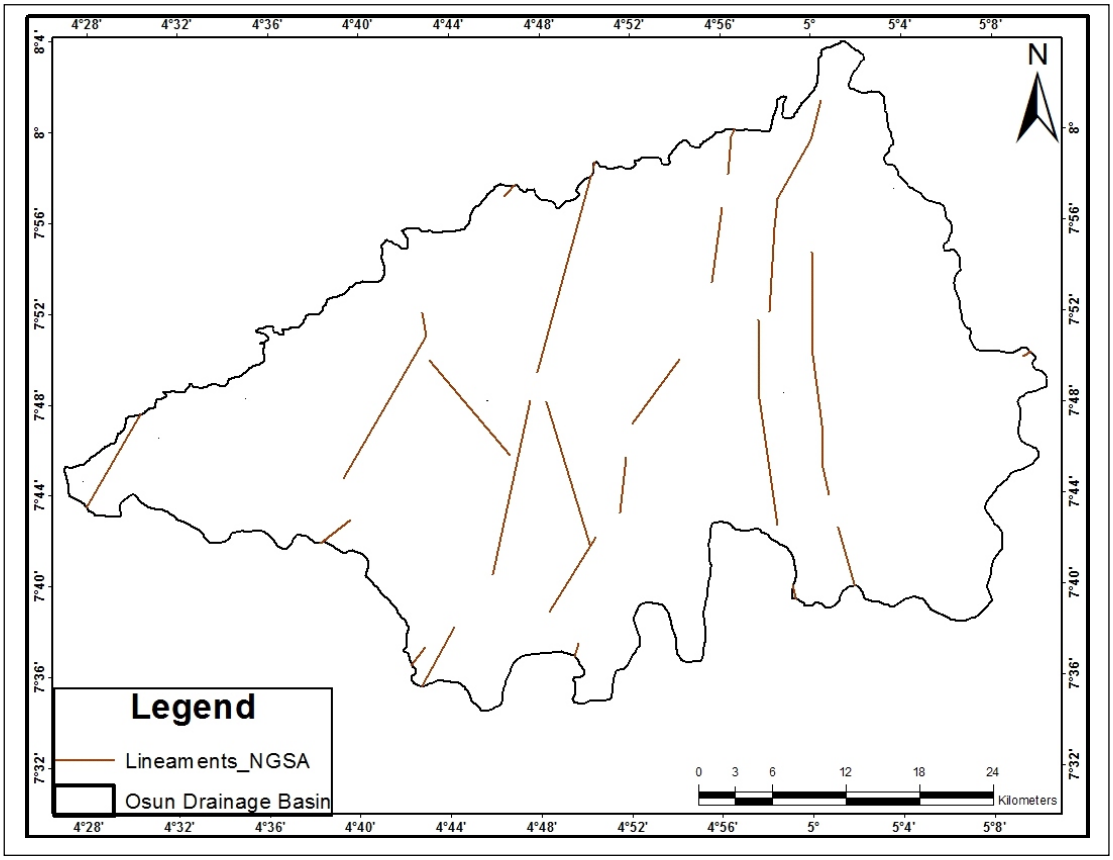

Figure 15a: Hydrolineaments and Lineament Intersection Map (NGSA, 2006)

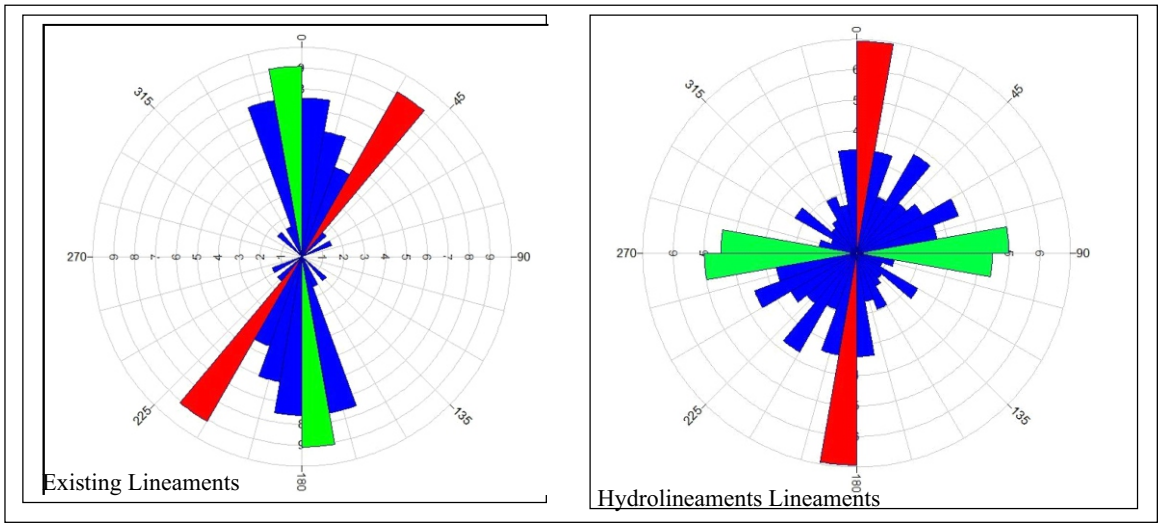

Figure 15b: Frequency-Rose Diagrams of Existing Lineaments and the Generated Hydrolineaments

Table 4: Pattern of Lineaments' Azimuth Directions

Azimuth Direction	N – S	NE – SW	NW – SE	E - W
Hydrolineaments (%)	2.44	62.19	33.34	2.03
Existing Lineament (%)	0	60	40	0

This study agrees with some previous studies on the efficiency of various optical images in lineament mapping. It was observed that the number of detected lineaments was higher for SPOT DEM (with 20 m Ground Survey Distance (GSD)) compared to ASTER DEM that has higher Ground Survey Distance (30 m GSD). Also, this study revealed that more lineaments were detected in the DEMs in contrast to fewer lineaments that were extracted from Landsat data. These facts have been emphasized by Mallast *et al.* (2011). Results showed that directional filter method is more suitable than non-linear filtering modules (such as Prewitt and High Pass) for edge enhancement. In this case, the efficiency of directional filters as a preferred edge enhancement method has been emphasized by Wladis (1999), Pratt (2007) and Mallast *et al.* (2011). The overall assessment of the two lineament procedures adopted in this study showed that PCI LINE is far better than Imagine Objective line extraction procedure in terms of speed, efficiency, and reliability of the final output (Mallast *et al.,* 2011). As earlier observed by Awoyemi *et al.* (2005) and Bayowa (2013), this study affirmed that the major lineament strikes in the study area constitute NE-SW (representing Zungeru – Ifawara mega fault line) and N-S orientations. And that the occurrence of lineaments varies with lithology across the study area.

On the other hand, the adoption of multiple datasets and the implementation of various techniques in this study have resulted in the delineation of new lineaments (particularly the near E-W oriented lineaments). Also, this study demonstrated the advantage of adopting 8-cardinal directional filtering when the aim is to delineate extensive lineaments that represent regional structures. Moreover, the adopted methodology enabled multiple confirmations of geological lineaments in the study area.

CONCLUSION

The automated approach was employed to extract lineaments from Digital Elevation Models (SPOT DEM and ASTER DEM) and Landsat OLI (band 6). In order to achieve the best result, various image enhancement techniques were adopted. Although all the adopted image enhancement techniques yielded positive results but finer details were enhanced in directional filtered images. In the same vein, the Object-based automated approach of PCI LINE was found to be highly efficient compared to the semi-automated approach of the Imagine Objective linear feature extraction procedure. However, Imagine Objective procedures demonstrated an unusually efficiency in restricted azimuth directional lineament extractions. It was observed that the number of lineament increases with decreased azimuth interval of filtering directions with SPOT DEM giving the highest number of lineaments.

Directional filtering along N-S and E-W directions proved to be the most efficient in detecting most lineaments within the study area. The image data on which the directional filter was applied is as important as the filter directions. The regional and local features with prominent trends were conspicuously enhanced in SPOT DEM outputs than in ASTER DEM and Landsat image due to its finer spatial resolution. However, minor but hydrogeologically significant lineaments were better captured in Landsat outputs. Analyses showed that the dominant azimuth directions of lineaments are NE-SW and NW-SE while minor trends consist of N-S and E-W orientations. Results showed that the adoption of multiple datasets and techniques would ensure the generation of reliable lineament map particularly in Basement Complex terrain. Moreover, SPOT DEM proved to be the most efficient among the input digital datasets.

Results showed that only 47.5 percent of the composite lineaments were hydrogeologically significant with dominant azimuth directions of NE-SW and N-S while minor trends such as NW-SE and E-W were also represented. The clustering of hydrogeologically significant lineaments and corresponding lineament intersections coincided with the occurrence of felsic rocks (quartzite/quartz schist and granitic rock) particularly within the upland axis of the study area. The newly generated lineament map agreed with the existing lineament map of the study area. However, the newly generated lineament map suggests the existence of other geological structures that have not been confirmed on the ground. In conclusion, the reliability of a

lineament map is largely dependent on the spatial and spectral resolution of the input remotely sensed datasets as well as the competence of the adopted techniques.

REFERENCES

Akinluyi, F. O. 2013. Integration of Remotely Sensed and Geophysical Data in Groundwater Potential Evaluation of the Basement Complex Terrain of Ondo State, Southwestern Nigeria. An *Unpublished Ph.D Thesis*, Dept. of Geology, OAU, Ile-Ife, Nigeria

Anisimova, O. and Koronovsky, N. 2007. Lineaments in the Central Part of the Moscow Syneclise and their Relations to Faults in the Basement. *Geotectonics.* Vol. 41(4) Pp. 315-332

Arenas Abarca, M. A. 2006. Lineament Extraction from Digital Terrain Models: Case Study of San Antonio del Sur Area, South-eastern Cuba. ITC, Enschede. 81Pp

Arias-Castro, E. and Donoho, D. L. 2009. Does Median Filtering Truly Preserve Edges better than Linear Filtering? *Annals of Statistics.* Vol. 37(3) Pp. 1172-1206

Awoyemi, M. O.; Onyedim, G. C.; Arubayi, J. B. and Ariyibi, E. A. 2005. Influence of Lithology and Geological Structures on Drainage Patterns in Part of the Basement Complex Terrain of Southwestern Nigeria. *Ife Journal of Science,* 7(2), 291-296

Bayowa, O. G. 2013. Hydrogeophysical Investigation of the Basement Complex Terrain of Ekiti State, Southwestern Nigeria. *An Unpublished Ph.D Thesis*, Dept. of Geology, OAU, Ile-Ife, Nigeria.

Boesse, T. N. and Ocan, O. O. 1988. Geology and Evolution of the Ife-Ilesa Schist Belt, Southwestern Nigeria. *Symposium on Benin-Nigeria Go-traverse of Proterozoic Geology and Tectonics of High Grade Terrains.*, 87-107

De Swardt, A. M. J. 1953. The Geology of the Area around Ilesa. *Geol. Surv. Nig. Bulletin* 23

Elueze, A. A. 1977. Geological and Geochemical Studies in the Ilesa Schist Belt in relation to the Gold Mineralization. *An Unpublished M. Phil. Thesis.* University of Ibadan.

Greenbaum, D. 1987. Lineament Studies in Masvingo Province, Zimbabwe, *British Geological Survey Report* WC/87/7.

Hobbs, W. H. 1904. Lineaments of the Atlantic Border Region. *Geol. Soc. Am. Bull.* Vol. 15 Pp. 483-506

Hung, L. Q., Batelaan, O. and De Smedt, F. 2005. Lineament Extraction and Analysis, Comparison of Landsat ETM and ASTER Imageries. Case Study: Suoimuoi Tropical Karst Catchment, Vietnam. *Remote Sensing for Environmental Monitoring, GIS Applications and Geology. V.SPIE, Brigge, Belgium*, 59830T-12

Jordan, G. and Schott, B. 2005. Application of Wavelet Analysis to the Study of Spatial Pattern of Morphotectonic Lineaments in Digital Terrain Models: A Case Study. *Remote Sens. Environ.* Vol. 94(1) Pp. 31-38

Kar, A. 1994. Lineament Control on Channel Behaviour during the 1990 Flood in the Southeastern Thar Desert. *Int. J. Rem. Sens.* Vol. 15 Pp. 2521-2530.

Karnieli, A., Meisels, A., Fisher, L. and Arkin, Y. 1993. Automatic Extraction and Evaluation of Geological Linear Features from Digital Remote sensing Data using a Hough Transform. *Proc. 9th Environmental Research Institute of Michigan thematic Conference on Geologic Remote Sensing, Pasadena, California.* Pp. 299-310

Koopmans, B. N. 1986. A Comparative Study of Lineament Analysis from Different Remote Sensing Imagery over Areas in the Benue Valley and Jos Plateau Nigeria. *Int. J. Rem. Sens.* Vol. 7 Pp. 1763-1771.

Lattman, L. H. 1958. Technique of mapping Geologic Fracture Traces and Lineaments on Aerial Photographs. *Photogrammetric Engineering*, 19 (4), 568-576.

Lattman, L. H. and Parizek, R. R. 1964. Relationship between fracture traces and the occurrence of groundwater in carbonate rocks. *Journal of Hydrology*, 2, 73-91.

Mallast, U.; Gloaguen, R.; Geyer, S.; Rodiger, T. and Siebert, C. 2011. Semi-Authomatic Extraction of Lineaments from Remote Sensing Data and the Derivation of Groundwater Flowpaths. *Hydrol. Earth Syst. Sci. Disc.,* 8, 1399-1431

Mather, P. M. 2004. Computer-Processing of Remotely-Sensed Images: An Introduction. West Sussex, UK. Pp. 324

Meijerink, A. M. J., Bannert, D., Batelaan, O., Lubczynski, M. W. and Pointet, T. 2007. Remote Sensing Applications to Groundwater. *IHP-VI Series on Groundwater*. UNESCO, Paris. Pp.311

Moore, G. K. and Waltz, F. A. 1983. Objective Procedures for Lineament Enhancement and Extraction. *Photogrammetric Engineering and Remote Sensing*. Vol. 87 Pp. 641-647

Nigeria Geological Survey Agency 2006. The Geological Map of Nigeria. NGSA. Abuja.

O'Leary, D. W., Friedman, J. D. and Pohn, H. A. 1976. Lineaments, Linear, Lineations: Some Proposed New Standards for Old Terms. *Geol. Soc. Am. Bull.* Vol 89. Pp. 1463-1469

Odeyemi, I .B.; Anifowose, Y. B. and Asiwaju-Bello, Y. A. 1999. Multi-Technique Graphical Analyses of Fractures from Remote Sensing Images of Basement Regions of Nigeria. *J. Min. Geol.,* 35(1), 9-21

Oguchi, T., Aoki, T. and Matsuta, N. 2003. Identification of an Active Fault in the Japanese Alps from DEM-based Hill Shading. *Comp. Geosci.* Vol. 29(7) Pp.885-891

Ojo, J. S., Olorunfemi, M. O., Akintorinwa, O. J., Bayode, S., Omosuyi, G. O. and Akinluyi, F.O. 2015. GIS Integrated Geomorphological, Geological and Geoelectrical Assessment of the Groundwater Potential of Akure Metropolis, Southwest Nigeria. *J. Earth Sci. Geotecn. Eng. Vol.* 5(14). Pp. 85-101

Oluyide, P. O. 1988. Structural Trends in the Nigerian Basement Complex. In Oluyide, P. O., Mbonu, W. C., Ogezi, A. E., Egbuniwe, I. G., Ajibade, A. C., and Umeji, A. C. (Eds.): Precambrian Geology of Nigeria. *Geol. Surv. Nigeria*, 99 – 102

Philip, G. 1996. Landsat Thematic Mapper Data Analysis for Quaternsry Tectonics in parts of the Doon Valley, NW Himalaya, India. *Int. J. Remot. Sens.* Vol. 17(1) Pp. 143-153

Quackenbush, L. J. 2004. A Review of Techniques for Extracting Linear features from Imagery. *Photogramm. Eng. Rem. S*. Vol. 70(12) Pp. 1383-1392

Salvi, S. 1995. Analysis and Interpretation of Landsat Synthetic Stereo Pair for the Detection of Active Fault Zones in the Abruzzi Region, Central Italy. *Rem. Sens. Environ*. Vol. 53(3) Pp. 153-163

Sander, P. 2007. Lineaments in Groundwater Exploration: A Review of Applications and Limitations. *Hydrog. J.* Vol. 15(1) Pp 71-74

Sander, P. 2007. Lineaments in Groundwater Exploration: A Review of Applications and Limitations. *Hydrogeol. J.* Vol. 15(1) Pp. 71-74

Sander, P., Minor, T. B. and Chesley, M. M. 1997. Groundwater Exploration based on Lineament Analysis and Reproductivity tersts. *Groundwater*. Vol. 35(5) Pp. 1-7

Solomon, S. 2003. Remote Sensing and GIS: Applications for Groundwater Potential Assessment in Eritrea. *A Ph.D Thesis* Submitted to the Department of Environmental and Natural Resources Information Systems, Royal Institute of Technology. Sweden. 137pp

USGS 2015. Landsat 8 (L8) Data Users Handbook. *EROS*, Sioux Falls, South Dakota. USA

Vaz, D. A., Di Achille, G., Baratta, M. T. and Alves, E. I. 2008. Manual and Automatic Lineament Mapping: Comparing Results. *Lunar and Planetary Science*. XXXIX

Wang, J. and Howarth, P. J. 1990. Use of the Hough Transform in Automated Lineament Detection. IEEE Trans. *On Geoscience and Remote Sensing*. Vol. 28(4) Pp. 561-566

Wladis, D. 1981. Automatic Lineament Detection using Digital Elevation Models with Second Derivative Filters. *Photogramm. Eng. Rem. S*. Vol. 65(4) Pp. 453-458